Endothelial cell CD36 optimizes tissue fatty acid uptake

Ni-Huiping Son, Debapriya Basu, Dmitri Samovski, Terri A. Pietka, Vivek S. Peche, Florian Willecke, Xiang Fang, Shui-Qing Yu, Diego Scerbo, Hye Rim Chang, Fei Sun, Svetlana Bagdasarov, Konstantinos Drosatos, Steve T. Yeh, Adam E. Mullick, Kooresh I. Shoghi, Namrata Gumaste, KyeongJin Kim, Lesley-Ann M. Huggins, Tenzin Lhakhang, Nada A. Abumrad, Ira J. Goldberg

Research In-Press Preview Endocrinology Metabolism

Movement of circulating fatty acids (FAs) to parenchymal cells requires their transfer across the endothelial cell (EC) barrier. The multi-ligand receptor cluster of differentiation 36 (CD36) facilitates tissue FA uptake and is expressed in ECs and parenchymal cells such as myocytes and adipocytes. Whether tissue uptake of FAs is dependent on EC or parenchymal cell CD36, or both, is unknown. Using a cell-specific deletion approach, we show that EC, but not parenchymal cell CD36 deletion increased fasting plasma FAs and postprandial triglycerides. EC-*Cd36* knockout mice had reduced uptake of radiolabeled long chain FAs into heart, skeletal muscle, and brown adipose tissue; these uptake studies were replicated using [^{11}C]palmitate PET scans. High fat diet-fed EC-CD36 deficient mice had improved glucose tolerance and insulin sensitivity. Both EC and cardiomyocyte (CM) deletion of CD36 reduced heart lipid droplet accumulation after fasting, but CM deletion did not affect heart glucose or FA uptake. Heart expression of several genes modulating glucose metabolism and insulin action increased with EC-CD36 deletion, but decreased with CM deletion. In conclusion, EC CD36 acts as a gatekeeper for parenchymal cell FA uptake, with important downstream effects on glucose utilization and insulin action.

Find the latest version:

Endothelial Cell CD36 Optimizes Tissue Fatty Acid Uptake

Authors: Ni-Huiping Son[1], Debapriya Basu[1], Dmitri Samovski[2], Terri A. Pietka[2], Vivek S. Peche[2], Florian Willecke[1], Xiang Fang[1], Shui-Qing Yu[1], Diego Scerbo[1], Hye Rim Chang[1], Fei Sun[1], Svetlana Bagdasarov[1], Konstantinos Drosatos[3], Steve T. Yeh[4], Adam E. Mullick[4], Kooresh I. Shoghi[5], Namrata Gumaste[1], KyeongJin Kim[6], Lesley-ann Huggins[1], Tenzin Lhakhang[7], Nada A. Abumrad[2*], Ira J. Goldberg[1*]

Affiliations:

[1]Division of Endocrinology, Diabetes and Metabolism, New York University School of Medicine, New York, NY 10016.

[2]Department of Medicine, Washington University School of Medicine, St. Louis, MO 63110.

[3]Department of Pharmacology, Lewis Katz School of Medicine at Temple University, Philadelphia, PA 19140.

[4] Ionis Pharmaceuticals, Inc., Carlsbad, CA, 92010.

[5] Department of Radiology, Washington University School of Medicine, St Louis, MO 63110.

[6] Division of Endocrinology, Columbia University Medical Center, New York, NY 10032.

[7]NYU Genome Technology Center, NYU Langone Medical Center, New York, NY 10016.

*Correspondence to:
Ira J. Goldberg, M.D.
Division of Endocrinology, Diabetes and Metabolism
NYU Langone Medical Center
Science Building 617
435 E. 30th Street
New York, NY 10016, USA
Phone: 646 501-0589; Fax: 212 263-9497
Email: Ira.Goldberg@nyumc.org
Or
Nada A. Abumrad, Ph.D.
Department of Medicine, Washington University School of Medicine
660 S Euclid Avenue, Campus Box 8031
St. Louis, MO 63110, USA
Phone: 314 747-0348
Email: Nabumrad@wustl.edu

Conflict of Interest Statement: The authors have declared that no conflict of interest exists.

Abstract: Movement of circulating fatty acids (FAs) to parenchymal cells requires their transfer across the endothelial cell (EC) barrier. The multi-ligand receptor cluster of differentiation 36 (CD36) facilitates tissue FA uptake and is expressed in ECs and parenchymal cells such as myocytes and adipocytes. Whether tissue uptake of FAs is dependent on EC or parenchymal cell CD36, or both, is unknown. Using a cell-specific deletion approach, we show that EC, but not parenchymal cell CD36 deletion increased fasting plasma FAs and postprandial triglycerides. EC-*Cd36* knockout mice had reduced uptake of radiolabeled long chain FAs into heart, skeletal muscle, and brown adipose tissue; these uptake studies were replicated using [^{11}C]palmitate PET scans. High fat diet-fed EC-CD36 deficient mice had improved glucose tolerance and insulin sensitivity. Both EC and cardiomyocyte (CM) deletion of CD36 reduced heart lipid droplet accumulation after fasting, but CM deletion did not affect heart glucose or FA uptake. Heart expression of several genes modulating glucose metabolism and insulin action increased with EC-CD36 deletion, but decreased with CM deletion. In conclusion, EC CD36 acts as a gatekeeper for parenchymal cell FA uptake, with important downstream effects on glucose utilization and insulin action.

Introduction

Long-chain fatty acids (LCFAs) provide cellular energy and are precursors for membrane components and intracellular lipid stores. Their bioactive derivatives influence gene expression and signal transduction pathways. Distribution of LCFAs among organs, especially muscle, adipose, and liver, is key to maintaining metabolic homeostasis (1). In the bloodstream, LCFAs circulate as unesterified "free" fatty acids (FFAs) bound to albumin or as triglyceride (TG) and phospholipid components of lipoproteins. Tissue uptake of LCFAs requires transfer across an endothelial cell (EC) barrier, but the molecular events necessary for this remain unknown.

In cultured parenchymal cells, LCFA uptake occurs via a saturable receptor-mediated pathway and a non-saturable pathway thought to reflect passive diffusion (2, 3). Several proteins have been implicated in facilitating LCFA accumulation, including enzymes involved in fatty acid (FA) acylation and the scavenger receptor cluster of differentiation 36 (CD36) (4). CD36 (also called SR-B2) is a multifunctional protein involved in apoptotic cell uptake, signal transduction, cellular adhesion, angiogenesis, and immune function (5). It was first linked to lipid metabolism when it was shown to function as a macrophage receptor for oxidized LDL (6) and as an adipocyte receptor/transporter for LCFAs (7). LCFA binding to the CD36 ectodomain is followed by FA transfer to the plasma membrane through an internal tunnel that runs the length of the protein, as shown by the crystal structure of the CD36-LCFA complex (8). CD36 also functions as a LCFA sensor, influencing activation of PPARs (9) and AMPK (10).

In mice, germline CD36 deficiency reduces acute accumulation of LCFAs in the heart, skeletal muscle, and adipose tissues (11). Moreover, $Cd36^{-/-}$ mice have increased fasting levels of FFAs (11, 12) and delayed clearance of postprandial lipids (11-13). The defect in LCFA uptake is also observed in CD36 deficient humans (14). Furthermore, a common haplotype at the CD36 locus associates with greater circulating FFA levels (15). Whether the defect in FA uptake is consequent to reduced CD36 expression in ECs, parenchymal cells, or both is unknown. We created mice with CD36 deletion specific to ECs (EC-$Cd36^{-/-}$) or cardiomyocytes (CM-$Cd36^{-/-}$) to determine

3

which cell type(s) regulates organ/tissue accumulation of LCFAs and TGs. Our data show that EC CD36 is needed for optimal movement of LCFAs from the circulation to cardiomyocytes (CMs). LCFA uptake was also diminished in brown adipose tissue (BAT) and skeletal muscle, but not liver, of EC-$Cd36^{-/-}$ mice. Loss of EC CD36 improved glucose tolerance and insulin sensitivity, and increased glucose uptake during fasting in heart, muscle, and white adipose tissue (WAT). The data reveal that CD36-mediated FA transport across ECs rate-limits tissue FA uptake, and its loss leads to metabolic effects in parenchymal cells.

Results

CD36 is abundantly expressed in vascular ECs and CMs in human and mouse hearts.

We investigated CD36 distribution in human and mouse heart tissues and assessed fidelity of our cell-specific deletions. CD36 was present in ECs and CMs in both human and mouse hearts (Figure 1A); staining was most intense in small blood vessels, weaker in larger arteries, and absent in total $Cd36^{-/-}$ mouse hearts. In wild type (WT) mouse hearts subjected to Langendorff perfusion and subsequent sub-organ fractionation using gradient density separation and FACS, $Cd36$ mRNA levels were significantly higher in ECs than in CMs from both males (Figure 1B) and females (Figure S1A). *In situ* hybridization data showed $Cd36$ mRNA expression in WT, but not total $Cd36^{-/-}$ mouse hearts, with most intense signals in capillary ECs (Figure S1B).

CD36 mRNA and protein are specifically reduced in EC- and CM-$Cd36^{-/-}$ mouse hearts.

To determine contribution of EC versus CM CD36 to heart FFA uptake, we created a $Cd36^{flox/flox}$ mouse line (Figure 1C). We crossed $Cd36^{flox/flox}$ mice with Tie2-Cre mice to make EC-$Cd36^{-/-}$ mice and with MHC-Cre mice to make CM-$Cd36^{-/-}$ mice. Both groups were fertile and appeared normal. PCR was used to detect $Cd36^{flox/flox}$ and $Cd36^{-/-}$ alleles from tail (Figure 1D) and heart (Figure 1E) DNA. PCR product sequencing from $Cd36$ null fragments showed ablation of exons 3 and 4 of the $Cd36$ gene after Cre-mediated recombination (Figure 1F). $Cd36$ mRNA and protein were reduced >50% in hearts of EC-$Cd36^{-/-}$ mice, compared to $Cd36^{flox/flox}$ mice; CM-$Cd36^{-/-}$ mice also had ~50% reduction of $Cd36$ mRNA in the heart with parallel reductions in protein content (Figure 1G). The approximately 50% reduction with either the EC or CM knockout suggests that total heart CD36 is equally divided into these two cell types. EC-$Cd36^{-/-}$ mice had reduced CD36 mRNA in skeletal muscle, BAT, and liver (Figures S1C -S1E) and parallel reductions in CD36 protein were measured in skeletal muscle, adipose tissues (white and brown), and liver (Figure 1H). Immunohistologic analysis of cardiac ventricular sections stained with polyclonal rabbit CD36 antibody confirmed CD36 ablation specificity to capillary ECs of EC-$Cd36^{-/-}$ mice (Figure 2A). These mice had significantly reduced CD36 in the lungs, which are particularly rich in ECs (Figure

5

S1F). To verify that CD36 is specifically deleted in ECs, we double stained EC-$Cd36^{-/-}$ heart tissues with CD36 and the EC marker CD31. Both CD36 and CD31 co-localized to capillary ECs of $Cd36^{flox/flox}$ controls, while CD36 protein was undetected in CD31 positive EC-$Cd36^{-/-}$ heart tissues (Figure 2B). We further confirmed specificity of the EC versus CM deletions by immunofluorescence of isolated ECs and CMs from lung and heart tissues. CMs from EC-$Cd36^{-/-}$ hearts contained normal amounts of CD36 protein, whereas CD36 was undetectable in those from CM-$Cd36^{-/-}$ hearts (Figure 2C). Primary ECs, isolated from lungs of $Cd36^{flox/flox}$ and EC-$Cd36^{-/-}$ mice, were stained for both VE-cadherin, an endothelial-specific molecule, and CD36 and showed absence of CD36 staining in VE-cadherin positive ECs from EC-$Cd36^{-/-}$ (Figure 2D).

To verify that $Cd36$ EC deletion did not cause off-target effects, we confirmed CD36 presence in CMs isolated from EC-$Cd36^{-/-}$ mice, analyzed by western blotting and quantitative real-time PCR (qRT-PCR) (Figure S1G). These data proved that CD36 was deleted in ECs but not parenchyma.

To determine whether CD36 deletion modified the metabolic gene profile in ECs, we isolated ECs from $Cd36^{flox/flox}$, EC-$Cd36^{-/-}$, and CM-$Cd36^{-/-}$ mouse hearts using FACS. Genes involved in glucose metabolism were not altered significantly in ECs from the three groups (Figure S1H). We also found no changes in FA oxidation genes in ECs with CD36 deletion, consistent with glucose being the primary substrate for ATP production in these cells. Thus, CD36 is not a major regulator of lipid or glucose metabolism in ECs.

We used laser capture microdissection (LCM) technology to isolate CMs and determine expression of glucose and FA metabolism genes. $Glut1$ mRNA increased, while pyruvate dehydrogenase kinase 4 ($Pdk4$) and carnitine palmitoyl transferase 1 ($Cpt1$) were decreased in the EC-$Cd36^{-/-}$ CMs (Figure S1I). These changes suggest a switch from FA to glucose use.

CD36 deletion in ECs increases plasma FFA and postprandial TG levels, while decreasing plasma glucose levels and enhancing insulin sensitivity.

Deletion of EC *Cd36* increased fasting plasma FFAs (Figure 3A), a phenotype similar to that of mice with global CD36 deletion (12). Fasting plasma total cholesterol (TC), TG, glycerol, and lipoprotein lipids (Figures S2A-E) were unchanged in 4-month old male EC-*Cd36*$^{-/-}$ as compared to *Cd36*$^{flox/flox}$ controls. However, age-matched female EC-*Cd36*$^{-/-}$ mice showed decreased plasma glucose together with increased fasting plasma TC, FFA, and TG associated with an increase in VLDL-TG and HDL-TC (Figure S3A-F). These sex-differences in lipid levels might reflect previously reported gender differences in regulation of tissue CD36 expression and muscle FA metabolism (16, 17). Loss of CD36 in CMs did not alter circulating levels of FFAs or glucose (Figure 3A and 3B). Therefore, loss of CD36 only in ECs reproduced many of the overall metabolic effects seen with total body CD36 knockout.

Postprandial TG levels in response to fat intake were higher in EC-*Cd36*$^{-/-}$ mice. Plasma TG levels at 2, 4 and 6 h post olive oil gavage were higher in EC-*Cd36*$^{-/-}$ compared to *Cd36*$^{flox/flox}$ mice (Figure 3C). Area under the curve for TG clearance (AUC$_{TG}$) showed a more than 2-fold increase in EC-*Cd36*$^{-/-}$ mice (Figure 3C insert table), suggesting that EC CD36 is involved in rapid clearance of circulating TGs. In contrast, loss of CM CD36 did not alter TG excursion (Figure 3C). Slower postprandial TG clearance is characteristic of total CD36 deficiency in mice (13) and humans (18) and may reflect greater product inhibition of lipoprotein lipase (LpL) by FFAs.

Glucose levels and insulin sensitivity are altered by loss of CD36 in ECs.

EC-*Cd36*$^{-/-}$ mice had decreased fasting (16 h) glucose levels, and improved oral glucose tolerance (OGTT) (Figure 3D), as was previously found in total *Cd36* knockouts (19). AUC for OGTT (AUC$_{OGTT}$) for EC-*Cd36*$^{-/-}$ mice was 24% lower than for *Cd36*$^{flox/flox}$ mice (Figure 3D insert table). Insulin tolerance tests (ITT) in 2 h fasted mice showed that more rapid glucose removal was due to greater insulin sensitivity (Figure 3E).

We generated a second endothelial knockout line by crossing *Cd36*$^{flox/flox}$ with VE-cadherin-Cre (VE-*Cd36*$^{-/-}$). In this model, plasma glucose was decreased while FFAs were increased, similar to the effects seen in Tie2-Cre EC-*Cd36*$^{-/-}$ mice (Figure S4A, B).

7

To confirm that the changes in FFA and glucose levels were not due to off target CD36 deletion, we created myeloid CD36 knockout mice using the LysM-Cre transgene. The deletion did not reduce glucose or increase circulating FFA levels (Figures S5A and S5B).

CD36 deletion in ECs improved glucose homeostasis and improved insulin sensitivity in high fat diet (HFD)-fed mice.

We next determined whether EC-CD36 loss affected FFAs and glucose in HFD-fed mice. EC CD36 deletion did not change body weight compared to controls (Figure 4A). As with chow, HFD-fed EC-$Cd36^{-/-}$ mice had higher circulating FFA levels (Figure 4B). These mice also had higher plasma TC and TG levels (Figures 4C and 4D), due to increases in both LDL and HDL cholesterol (Figures S5C).

Total body $Cd36^{-/-}$ mice fed HFD had improved insulin sensitivity (19). HFD-fed EC-$Cd36^{-/-}$ mice had lower glucose and insulin concentrations (Figures 4E and 4F) and improved OGTT (Figure 4G) and ITT (Figure 3H). Because we had seen such prominent changes in gene expression in the heart, we assessed insulin signaling after a fasting/feeding episode. After fasting and refeeding, EC-$Cd36^{-/-}$ hearts had greatly increased phosphorylation of AKT (p-AKT) and the ribosomal protein S6 (S6) at serine 240/244 (p-S240/244), both downstream targets of insulin signaling (Figures 4I), whereas heart insulin receptor (IR) phosphorylation did not change. To further assess insulin sensitivity, muscle, liver, and WAT were obtained after insulin injection. In EC-$Cd36^{-/-}$ liver, phosphorylation of IR (p-IR) was significantly increased (Figure 4J). Deletion of $Cd36$ in ECs did not change IR, AKT, and S6 protein levels in skeletal muscle and WAT (Figures 4K and S5D). To test whether improved insulin sensitivity in HFD EC-$Cd36^{-/-}$ mice was related to reduction of ceramides and diacylglycerols (DAGs), we determined distribution of these lipids in skeletal muscle and hearts. Long-chain ceramides (Cer 18:1) in the heart and very long-chain ceramides (Cer22:0, Cer24:0 and Cer24:1) in both heart and skeletal muscle were significantly reduced in EC-$Cd36^{-/-}$ mice (Figures 4L and 4M). Cardiac and muscular DAGs were not altered

8

(Figures S5E and S5F). Thus, EC-CD36 deletion protected from HFD-induced insulin resistance and associated with reduced ceramide species.

CD36 deletion in ECs reduces LCFA uptake by heart, skeletal muscle, and BAT.

To test directly whether loss of CD36 in ECs reduced uptake of LCFAs *in vivo*, we injected [³H]oleic acid and [¹⁴C]hexanoic acid, which is not recognized by CD36, into 16 h fasted male mice and assessed their tissue uptake. Compared to *Cd36^flox/flox* and CM-*Cd36^-/-* mice, EC-*Cd36^-/-* mice had significantly delayed plasma clearance of oleic acid (Figure 5A) and a >50% reduction in oleate uptake by heart, quadriceps muscle, and BAT (Figure 5B). In contrast, uptake by liver, lung, and kidney was unchanged. Similar results showing reduced plasma LCFA clearance and uptake into heart and BAT were observed in female mice (Figures S6A and S6B). However, skeletal muscle uptake was not altered in female mice. The lack of significant changes in skeletal muscle uptake in the females are consistent with the known gender differences in skeletal muscle lipid metabolism (20). The signal in WAT was low, and uptake differences were not significant. Hexanoic acid plasma removal and uptake into tissues were similar in all three genotypes (Figures 5C and 5D). These data show that EC-CD36 is required for optimal LCFA uptake by the heart, skeletal muscle, and BAT.

We also assessed acute LCFA accumulation in the heart and other tissues in real time using [¹¹C]palmitate PET. As found with radiolabeled tracers, EC-*Cd36^-/-* mouse hearts had a marked reduction in tracer uptake compared to *Cd36^flox/flox* and CM-*Cd36^-/-* mouse hearts (Figure 5E). Significantly reduced FA uptake by skeletal muscle and BAT was also measured in EC-*Cd36^-/-* mice (Figure 5F). In contrast to the reduction noted with EC deletion, both [³H]oleic acid (Figure 5B) and PET scan assessment of heart palmitate uptake (Figure 5E right panel) in CM-*Cd36^-/-* mice were not different from those in *Cd36^flox/flox* mice. Neither deletion affected palmitate uptake in the liver (Figure S6C).

CD36 deletion in ECs increases glucose uptake by heart, skeletal muscle, and BAT.

9

Fasting reduces glucose uptake by heart and muscle, an adaptation impaired by total CD36 deficiency in humans (21) and mice (4, 9). We examined tissue uptake of [^{18}F]deoxyglucose (FDG) using PET in 16 h fasted mice. Glucose uptake increased in heart, muscle, and WAT of EC-*Cd36*$^{-/-}$ mice as compared to controls (Figure 5G). In contrast, tissues of CM-*Cd36*$^{-/-}$ mice showed no changes in glucose uptake (Figure S6D). These data show that EC CD36 regulates the fasting-induced metabolic shift by tissues, which spares glucose use and increases reliance on FAs.

CD36 deletion in either ECs or CMs reduces heart lipid storage.

The heart normally increases its lipid stores during fasting. Studies in *Cd36*$^{-/-}$ mice suggest that CD36 is required for this adaptation (4, 9, 10, 22). We fasted mice for 16 h and assessed lipid droplet accumulation using BODIPY. Lipid droplet accumulation was significantly reduced in EC-*Cd36*$^{-/-}$ hearts (Figure 6A). Lipid droplet numbers were significantly decreased in both EC-*Cd36*$^{-/-}$ and CM-*Cd36*$^{-/-}$ hearts, assessed by electron microscopy (Figures 6B and 6C), while heart morphology appeared normal. Direct measurements of heart TG showed that hearts from EC-*Cd36*$^{-/-}$ had a 49% reduction in TG, and CM-*Cd36*$^{-/-}$ mice had a 53% reduction (Figure 6D). Thus, CD36 deletion in either ECs or CMs reduced heart lipid accumulation. Decreased cardiac lipid accumulation was also seen in VE-*Cd36*$^{-/-}$ mice (Figure S7A and S7B). As might be expected with reduced lipid uptake into peripheral tissues, EC-*Cd36*$^{-/-}$ mice had increased liver TG content (Figure S7C). The increased heart TG associated with increased diacylglycerol acyl transferase 1 (DGAT1) (Figure S1E), a compensation that might have prevented the accumulation of lipids that interfere with insulin signaling (23, 24).

EC or CM CD36 deletion reduce heart genes of FA metabolism and differentially alter those of glucose metabolism.

We performed RNA sequencing (RNA-Seq) to gain an unbiased global view of transcript expression in EC-*Cd36*$^{-/-}$ and CM-*Cd36*$^{-/-}$ mouse hearts. Gene heatmap analysis (Figure 7) showed marked expression changes in hearts from both mice groups. Expression of genes of

glucose metabolism and glucose signaling showed differential regulation. In EC-*Cd36*$^{-/-}$ mouse hearts, increases were observed in mRNAs of genes mediating glucose uptake and oxidation such as *Slc2a1* (Glut1), *Slc2a4* (Glut4), *Pcx* (pyruvate carboxylase), *Hk2* (hexokinase 2), *Gck* (glucokinase), and *Pfkfb2* (6-phosphofructo-2-kinase/fructose-2,6-biphosphatase 2). Decreased expression of *Pdk4* (pyruvate dehydrogenase kinase 4), which inhibits pyruvate conversion to acetyl-CoA, was consistent with enhanced glucose utilization. These changes were associated with increased expression of insulin signaling pathway genes such as *Irs1* (insulin receptor substrate 1), *Pten* (phosphatase and tensin homologue), *Pik3r1* (phosphoinositide 3 kinase regulatory subunit 1, p85), *Foxo1* (forkhead box protein 01) and *Mapk4* (mitogen activated protein kinase 4).

In hearts of *CM-Cd36*$^{-/-}$ mice, in contrast to *EC-Cd36*$^{-/-}$ mice, there was reduced cardiac expression of glucose metabolism genes, while genes for insulin signaling were not affected. These data suggest that CD36 deletion in ECs enhances expression of genes related to glucose utilization and insulin action while the effect of the deletion in CMs is opposite or neutral.

PPARs, especially PPARα, modulate LCFA oxidation in the heart. PPARα mRNA levels increased in EC-*Cd36*$^{-/-}$ hearts (Figure 6A red arrow), while PPARγ and β/δ were unchanged in both EC and CM knockout hearts. However, expression of genes of FA metabolism including many PPARα targets was decreased in both mice groups. For example *Slc27a1* (FA transport protein 1), *Cpt1a* (carnitine palmitoyl transferase 1a), *Cpt2*, *Acot2* (acyl CoA thioesterase 2), *Acadl* (acyl CoA hydrogenase 1), *Acadm* (medium chain ACAD) and *Hsd17b4* (hydroxysteroid 17 beta dehydrogenase 4), decreased significantly in EC-*Cd36*$^{-/-}$ and CM-*Cd36*$^{-/-}$ hearts. In both groups, *Slc25a20* (carnitine acyl carnitine translocase, *CACT*), which mediates the transport of acylcarnitines from the cytosol to the mitochondrial matrix, was reduced. These changes indicate that CD36 in both ECs and CMs regulates tissue FA metabolism. In CM-*Cd36*$^{-/-}$ hearts these changes are consistent with effects of CD36 on FA oxidation as documented in an overexpression mouse model (25) and in tissue culture experiments (26).

11

KEGG analyses of insulin- and PPAR-activated pathways highlighted enhanced insulin signaling in EC-*Cd36*$^{-/-}$ hearts with increased expression of major regulators of GLUT4 translocation, lipogenesis, and glycogenesis (Figure 8A). This was not apparent in CM-*Cd36*$^{-/-}$ hearts. There was diminished expression of major PPAR targets from EC-*Cd36*$^{-/-}$ (Figure 8B). Expression of several genes involved in the PPAR and insulin signaling pathways such as *Pparα* and *Glut1* were increased in hearts of EC-*Cd36*$^{-/-}$ mice, while *Fas* and *Ampk* expression were decreased (Figure 8C). Hearts from CM-*Cd36*$^{-/-}$ mice, like those from germline *Cd36*$^{-/-}$ mice, had higher *Ampk* mRNA levels (Figure S8A) (10, 22). This contrasted with lower *Ampk* levels in hearts from EC-*Cd36*$^{-/-}$ mice (Figure 8A), perhaps reflecting greater glucose uptake. However, like in EC-*Cd36*$^{-/-}$, expression of major PPAR target genes in CM-*Cd36*$^{-/-}$ was decreased (Figure S8B). These data were confirmed by qRT-PCR (Figure 8C). Decreased expression of *Pdk4, Cpt1*, and *Aox* mRNA was also found in female EC-*Cd36*$^{-/-}$ mouse hearts (Figure S8C).

Discussion

Delivery of LCFA to parenchymal cells in tissues that do not have fenestrated capillaries involves transfer from the circulation to parenchymal cells. This movement of LCFAs requires their transfer either through or around ECs. CD36 has been reported to mediate LFCA uptake into muscle and adipose tissues (11, 12) and LCFA accumulation in CMs (27) and other cells (28), but its role in ECs had not been directly studied. We show that ECs robustly express CD36 and EC-specific CD36 deletion reduces acute LCFA uptake into heart and other tissues. Moreover, EC-$Cd36^{-/-}$ mice have increased insulin sensitivity and lack myocardial lipid droplet accumulation with fasting. Reductions in ceramides might have contributed to the improved insulin sensitivity. The reduction in FA uptake into BAT might have important implications for thermogenesis. In this regard, Bartelt et al. (29) have shown that both LpL and CD36 affect BAT uptake of FAs during cold exposure.

A number of reports have suggested that ECs are a major regulator of tissue LCFA metabolism. These reports did not directly investigate EC CD36, but some included indirect evidence that is consistent with our current findings. Deletion of EC PPARγ increased circulating LCFAs (30) and reduced expression of several PPARγ gene targets in EC including CD36. Meox2/Tcf15 heterodimer transcription factors (TFs) in ECs have been reported to regulate FA transfer across the cardiac capillary endothelium (31) and to affect expression of FA metabolizing genes, including *Cd36*. Deletion of EC VEGF-B (32) was reported to cause changes in EC LCFA uptake due to transcriptional regulation of vascular-specific FA transport proteins 3 and 4, but this was not confirmed by others (33). A recent report showed that a metabolite of branch chain amino acids modulated both LCFA movement across ECs and also insulin sensitivity (34). Interestingly, the molecular mechanisms mediating FA uptake by EC CD36 might differ between tissues; Salameh et al. recently reported on a mechanism specific to adipocytes. They described a prohibitin and annexin A2 complex that increases CD36 on the cell surface and FA uptake by ECs and adipocytes (35).

Robust CD36 expression in capillary ECs (36) is found in tissues that are most active in circulating LCFA extraction and that also express LpL and its EC anchoring protein GPIHBP1 (glycosylphosphatidylinositol anchored high density lipoprotein binding protein 1). This expression pattern suggests that CD36 is important in LCFA trafficking across smaller blood vessels and capillaries, where most nutrient uptake occurs. ECs are not major sites of FA oxidation, so CD36 in capillaries is likely to be more important for LCFA transport than for LCFAs derived ATP production. This conclusion is supported by our data showing that lack of CD36 expression does not change EC mRNA levels of genes for FA or glucose metabolism.

The lack of lipid droplet accumulation with EC and CM CD36 deletion shows that CD36 expression in both sites is required for optimal delivery of LCFAs to the heart. The defect in uptake in EC-$Cd36^{-/-}$ was evident using two types of tracer kinetic studies, radiolabeled LCFA and [^{11}C]palmitate PET. Both of these techniques assess the rapid accumulation of LCFAs and for this reason might have failed to show a defect in LCFA uptake in CM-$Cd36^{-/-}$ hearts; CM CD36 is well established to mediate LCFA accumulation in cultured CMs (37, 38), and to provide substrates required for response to acute afterload (39). In addition, our studies highlight important differences in the contribution of ECs versus CMs to FA metabolism in the heart, and additional studies are needed to understand the mechanisms underlying these differences.

Loss of EC CD36 led to improved insulin action and glucose disposal, demonstrated using cardiac gene expression, OGTT and ITT. These effects were confirmed in HFD-fed mice. Improvements in OGTT and ITT were similar to those observed with PPARα (40) or GLUT4 deletion (41). In addition, circulating glucose levels were reduced, as was found with some (42), but not all (43), genetic mutations that reduce FA oxidation. FDG PET showed increased glucose uptake into heart, skeletal muscle, and WAT with EC CD36 deletion. CM-$Cd36^{-/-}$ mice did not have similar improvements in insulin action or glucose metabolism, and instead hearts from these mice had downregulated expression of some glucose uptake genes, opposite to what would be expected with reduced lipid uptake. These changes might reflect myocyte autonomous actions of

14

CD36 that regulate insulin signaling (Samovski et al., Diabetes, in press). These separate effects on parenchymal biology are likely to explain the propensity to develop insulin resistance in humans with CD36 mutations (44).

In humans, CD36 deficiency has a prevalence of 0.3-9%, with higher incidence in Asian and African populations. Individuals with complete CD36 deficiency have higher serum levels of fasting TGs (45) and chylomicron remnants (18). These lipid abnormalities likely reflect defective tissue FA metabolism, as CD36 deficient individuals show markedly reduced LCFA uptake by the heart (14, 21) and have enhanced myocardial glucose uptake (21).

In summary, our data show that ECs are major sites of regulation of LCFA uptake and, in turn, tissue lipid metabolism and insulin sensitivity. By regulating heart and skeletal muscle FA delivery and glucose utilization, EC CD36 is a major factor affecting tissue fuel selection and systemic metabolism. Whether EC CD36 actions are beneficial for normal or diseased hearts is uncertain (46-48) and likely depends on the physiologic situation. Reduction of LCFA uptake will lead to impaired energy production during fasting or exercise, but will also protect from excess lipid accumulation (lipotoxicity) (49) and improve glucose utilization during hypoxia (50). The vascular endothelium represents an important and accessible therapeutic target (51) and our findings suggest that targeting EC CD36 could be a means to influence tissue FA uptake and prevent or treat a variety of diseases due to abnormal lipid utilization.

Methods

Generation of *Cd36*^{flox/flox} mice: A Lox (L83) site and Frt-Neo-Frt-Loxp (FNFL) cassette were engineered to flank a 1.7 kb sequence with exons 3 and 4 of CD36 to generate a "floxed/neo" CD36 allele on a bacterial artificial chromosome (BAC). A gene targeting vector was made by retrieving the 2 kb short homology arm (5' to L83), the floxed sequence containing exons 3 and 4, the FNFL cassette, and the 10 kb long homology arm (end of FNFL to 3') into a plasmid vector carrying a Diphtheria Toxin Alpha (DTA) chain negative selection marker. The FNFL cassette conferred G418 resistance during gene targeting in KV1 (129B6 hybrid) embryonic stem (ES) cells, and the DTA cassette provided autonomous negative selection to reduce random integration. Identified targeted ES cells were injected into C57BL/6 blastocysts to generate chimeric mice. Male chimeras were bred to homozygous ACTB (Flpe/Flpe) C57BL/6 females to remove the neomycin (NEO) cassette and transmit the floxed CD36 allele (Flpe recombinase). The mice were then crossed with Tie2-Cre and MHC-Cre mice (C57BL/6) to generate EC-*Cd36*^{-/-} and CM-*Cd36*^{-/-} mice and with LysM-Cre to create myeloid cell deficiencies. Founder *Cd36*^{flox/flox} mice were identified by tail genomic DNA analysis with primer 1F specific to the upstream loxp locus (5'- attggcatctgtgtagcgctcttggc-3'), and primer 1R (5'- tgctactatgcactccatgcaggc -3'), an antisense specific to the downstream loxp locus. *Cd36* deletion in the EC-*Cd36*^{-/-} heart was confirmed by PCR of heart tissue DNA and mRNA with primer 2 and 3 (Table 1), respectively. Mice were maintained under a constant light-dark cycle (light from 7:00 a.m. to 7:00 p.m.) and received either a standard diet (Labdiet Cat. 5053) or a HFD containing 65% fat (Research Diets Inc. Cat. D12492).

Human tissues: Normal human heart tissues were obtained from the Department of Surgery at Columbia University Medical Center.

Western blot analysis: Total proteins were obtained from fresh heart tissues of 4-6 month-old EC-*Cd36*^{-/-} and CM-*Cd36*^{-/-} mice and littermate controls using a RIPA kit (Santa Cruz). Proteins (30 μg), separated by Western blot, were probed for CD36 (AF2519 1:200 dilution; R&D) and α-

Tubulin (ab7291 1:5000 dilution; Abcam) as control. Antibodies against Akt (9272), p-Akt (S473, 4060), S6 (2217), p-S6 (S240/244, 2215), IR (3025), p-IR (3024) and β-actin (4970) were from Cell Signaling. Signals were quantified by densitometry using Odyssey® Fc Imaging System (LI-COR Biotechnology).

Heart and plasma lipids: Blood from fasted (4 or 16 h) mice was collected from the retro-orbital plexus. Plasma TC, TG, and FFA were measured enzymatically using an Infinity kit (Thermo Electron Corp.) and a NEFA C kit (Wako). To measure heart TG, hearts were perfused with PBS and homogenized at 4°C in 1 M NaCl buffer with lipase inhibitors. Lipids were extracted from heart tissues (50 mg) according to a modified Folch (52). The dried lipids were solubilized in PBS with 2% Triton X-100 and TG measured using an Infinity TG kit (Thermo Electron Corp.).

Immunohistochemistry: Human and mouse cardiac ventricular specimens were fixed in 10% buffered formaldehyde, embedded in paraffin and 5 µm-thick microtomic sections were stained with 1:100 dilution of mouse and human CD36 antibody (AF2519, AF1955; R&D). After washing, sections were incubated (2 h, room temperature) with a biotinylated rabbit anti-goat IgG antibody. Staining specificity was tested by omission of primary antibodies.

Immunofluorescence Staining: Cardiac ventricular tissues from 4-month old male mice were embedded in Tissue-Tek OCT compound (Sakura). Frozen sections (5 µm in thickness) were fixed in 10% formalin for 30 min, washed 3 times in PBS, and blocked for 1 h in 1% BSA-PBS at room temperature. The fixed sections were incubated (2 h, room temperature) with 1:100 dilution of either mouse CD36 (R&D, AF2519) and CD31 (Biolegend, 102514) antibodies followed by washing and incubations (1 h) with secondary antibody (1 : 500 dilution) coupled to Alexa dye 488 or 594 (Invitrogen). Washed sections were then stained with ProLong™ Gold Antifade Mountant with DAPI (Thermo Fisher Scientific) and digital images obtained with a Leica confocal microscope. Isolated ECs were fixed with 4% PFA, permeabilized with 0.2 % Triton X-100 and blocked with donkey serum. Then cells were incubated with anti-VE-cadherin (ab33168) and CD36 (AF2519) antibodies followed by secondary antibodies conjugated with Alexa Fluor 488

and Alexa Fluor 594. Nuclei were visualized with DAPI. Imaging used a Nikon Eclipse inverted microscope at 60X.

Lipoprotein isolation: Plasma was pooled from EC-*Cd36*$^{-/-}$ mice fed with chow and HFD. Lipoprotein fractions were separated by a previously described method (53).

OGTT: 16-h fasted *Cd36*$^{flox/flox}$, EC-*Cd36*$^{-/-}$, and CM-*Cd36*$^{-/-}$ mice were given 2 g of glucose/kg body mass intragastrically. Tail blood samples were collected and glucose measured at 0, 15, 30, 60, and 120 min post-gavage.

Plasma insulin measurement: *Cd36*$^{flox/flox}$ and EC-*Cd36*$^{-/-}$ were fasted for 16 h refed for 2 h. Blood was collected from the retro-orbital plexus, and plasma insulin measured using mouse ultrasensitive insulin ELISA kit (ALPCO).

ITT: Mice were fasted for 4 h, then given human insulin (Eli Lilly, 0.75 U/kg body weight) intraperitoneally. Tail blood was obtained at 0, 15, 30, 45, 60, and 120 min post-insulin injection.

Insulin signaling test: For insulin induced changes, insulin signaling was assessed in three-month old male mice with 6-week HFD using two different methods. Changes in the heart were most evident when assessed after fasting (16 h) followed by refeeding (2h), after which hearts were harvested and used for western blotting. Other tissues were studied after insulin injection (0.50 U/kg body weight of human insulin (Eli Lilly), IP). Skeletal muscle, liver, and WAT were harvested 20 min after insulin injection and used for western blotting.

Lipid droplet staining: Cardiac ventricular tissues from 4-month old male mice were embedded in Tissue-Tek OCT compound (Sakura). Frozen sections of myocardium (5 μm in thickness) were fixed in 10% formalin for 30 min at room temperature and then washed three times in PBS. The fixed sections were then incubated with 4 μM BODIPY™ 493/503 dye (Invitrogen Cat. No. D3922) for 30 min at room temperature. After washing, sections were stained with ProLong™ Gold Antifade Mountant with DAPI (Thermo Fisher Scientific) and covered with glass cover slips (VWR). The digital images were obtained with a Leica confocal microscope.

Postprandial lipemia: After a 16 h fast, mice maintained on a chow diet received an intragastric bolus of 0.3 ml of olive oil. Tail blood samples were collected before and at 2, 4, and 6 h post-gavage. Plasma TG concentration was assayed with an infinity kit.

EC isolation: Lungs harvested from *Cd36$^{flox/flox}$* and EC-*Cd36$^{-/-}$* mice (Tie2-Cre) were minced and enzymatically digested in MACS C-tube (Miltenyi Biotec). Cells were centrifuged, resuspended in PEB buffer (1x PBS, 0.5% BSA, 2mM EDTA), blocked with FcR blocking reagent (Miltenyi Biotec) then incubated with CD31 conjugated microbeads for 15 min at 4°C. The cell suspension was passed through MACS separation column, the column washed with PEB buffer (3X) and cells eluted and plated on gelatin-coated coverslips in 6 well plates.

Heart sub-organ fractionation: Cardiac cells were dissociated as described previously using Liberase TH (0.125 U/ml) (54). The cell suspension was filtered through a 100 μm strainer and centrifuged at 50g for 5 min. CMs were pelleted and subjected to Percoll density gradient centrifugation (1200g for 30 min) for RNA and protein isolation. Non-CMs in the supernatant were centrifuged at 500g (10 min) and prepared for FACS. RBCs in non-CMs were lysed and pellets resuspended in staining buffer (2% FBS/PBS, 2 mM EDTA, and 100U/ml RNase inhibitor, New England Biolabs, M0314L). Incubation with Calcein AM (100 nM, room temp, 30 min) then with CD45 and CD31 antibodies (BioLegend, 103114 and 102508) on ice (30 min) was followed by 7-AAD (5 μg/ml) addition 10 min before the end of the incubation. Cells were pelleted, resuspended, filtered (70 μm Flowmi cell strainer), and sorted on the FACSAria Fusion (BD Biosciences). Singlet cells were gated by FSC-A and FSC-H. Additional gating of live (Calcein AM+, 7-AAD-) cells was performed. CD45-, CD31+ EC fractions were collected for RNA isolation.

In situ **hybridization:** CD36 mRNA expression was detected in frozen sections via ISH using the QuantiGene ViewRNA tissue assay (Affymetrix) according to the manufacturer's instructions and probes. No probe controls or tissue from *Cd36* knockout mice were used for negative controls.

Laser capture microdissection (LCM): Mouse heart tissues were filled with O.C.T Compound. Polyethylene naphthalate (PEN) membrane glass slides were prepared and for cryosectioning.

The tissue block was cryosectioned entirely at 10 μm and stained with Hematoxylin and Eosin (H&E) staining for histomorphologic identification of cardiomyocytes. The Leica DM6000 B microscope was used for cardiomyocytes harvesting. The captured cardiomyocytes were subjected to RNA purification (Arcturus PicoPure RNA isolation kit, AB Applied Biosystem) and cDNA amplification (The Ovation® Pico WTA System V2, NuGEN).

Tissue gene expression: Mice (4 month old) were fasted for 16 h. Total RNA was prepared using a Pure Link Micro-to-Midi Total Purification kit (Invitrogen). 1 μg of RNA was treated with DNase I (Invitrogen) for 15 min and reverse transcribed using the ThermoScript RT-PCR Kit (Invitrogen). ABI 7700 (Applied Biosystems) and SYBR Green PCR Master Mix (Applied Biosystems) were used for qRT-PCR. Analysis used Sequence Detection Software (Applied Biosciences) and standard curves generated using undiluted and diluted (1:10, 1:100, and 1:1,000) cDNA heart tissue samples. Correlation coefficients were 0.98 or greater. Data were normalized to 18S rRNA.

RNA-Seq data analysis: Raw sequencing data were received in FASTQ format. Read mapping used Tophat 2.0.9 against the mm10 mouse reference genome. The resulting BAM alignment files were processed with the HTSeq 0.6.1 python framework and respective mm10 GTF gene annotation (UCSC database). The Bioconductor package DESeq2 (3.2) was used to identify differentially expressed genes (DEG) and for statistical analysis based on a negative binomial distribution model. The resulting values were adjusted using the Benjamini-Hochberg method for false discovery rate. Genes with an adjusted p-value < 0.05 were determined to be differentially expressed and KEGG Analysis was performed to identify top canonical pathways being altered. RNA sequencing data have been deposited in the GEO database. The accession number is GSE116350.

Electron microscopy: Left ventricles from 16-h fasted 4-month-old male mice were fixed with 2.5% glutaraldehyde, 2% paraformaldehyde in 0.1M sodium cacodylate buffer (pH 7.2) for 2 h, post-fixed with 1% osmium tetroxide (1.5 h, room temperature), processed and embedded in EMbed 812 (Electron Microscopy Sciences, Hatfield, PA). Ultrathin sections (60 nm) were cut

(Leica UC6 microtome), mounted on 200 mesh copper grids, and stained with uranyl acetate and lead citrate. Stained grids were examined with Philips CM-12 electron microscope and photographed with a Gatan (4k x2.7k) digital camera. Lipid droplets were counted in random $100\mu m^2$ areas.

Uptake of [^{3}H]oleic acid and [^{14}C]hexanoic acid: 16-h fasted 4-month-old $Cd36^{flox/flox}$, EC-$Cd36^{-/-}$, and CM-$Cd36^{-/-}$ mice were injected intravenously with 100 µl of PBS containing 1×10^6 DPM of [^{3}H]oleic acid and 1×10^6 of [^{14}C]hexanoic acid (PerkinElmer). Mouse plasma volume was estimated as 0.55 ml/kg body weight (55). Plasma radioactive concentration was calculated by body weight (mg) X (0.55 (ml)/1000 (mg)) X 10^6 (DPM). Blood was collected at 0, 30, 120, and 300 s post-injection for radioactive count (10 µl plasma). The heart vasculature was perfused with 10 ml PBS via cardiac puncture 5 min post-injection. Tissues were excised and accumulated radioactivity measured. Tissue oleic and hexanoic acid uptake was adjusted by plasma radioactivity at 30 min and normalized to littermate controls.

PET studies: Differences in FA metabolism and FDG were evaluated with PET imaging on 4-5 month old 16-h fasted mice using [^{11}C]palmitate and [^{18}F]DG as described previously (56). Uptake/transport of tracer was visualized and quantified by summing uptake kinetics up to 60 min post-tracer administration. All images and corresponding data were normalized to dose and weight of the animal and presented as standardized uptake value (SUV=activity X weight/injected dose).

Statistics: Results are expressed as mean $\pm$ SD. Significant differences between groups were determined by ANOVA t-test or one way ANOVA multiple comparisons analysis. AUC value was evaluated using Trapezoid method. A P value less than 0.05 was considered significant.

Study Approval: The IRB at Columbia University and New York University Medical Centers approved all study protocols. Creation of the mice and all metabolic and genetic studies were reviewed and approved by the New York University and Washington University IACUC.

Author Contributions:

N.S., N.A.A, and I.J.G. designed the study and wrote the manuscript.

N.S. created the targeting constructs for the genetically modified mice and performed experiments

assessing gene expression, plasma metabolites, and tissue analysis.

T.A.P. assisted with construct design and validation of the mice models.

F.W., X.F., and S.Y. performed the radioactive FA uptake experiments.

H.-R. C. created the LysM-Cre *Cd36*$^{-/-}$ mice and obtained data on their circulating lipid and glucose

levels.

D.B., D.S., T.A.P., S.T.Y., V.S.P, F.S., S.B., and L.H. performed experiments.

K.I.S. performed and analyzed the PET studies.

D.S. and T.L. contributed to data analysis and discussion.

K.D., A.E.M., and K.I.S. performed in situ hybridization and heart cell fractionation studies.

N.G. edited the manuscript.

K. K. assisted with western blotting for insulin signaling analysis

References

1. Stern JH, Rutkowski JM, and Scherer PE. Adiponectin, Leptin, and Fatty Acids in the Maintenance of Metabolic Homeostasis through Adipose Tissue Crosstalk. *Cell Metab.* 2016;23(5):770-84.

2. Sorrentino D, Robinson RB, Kiang CL, and Berk PD. At physiologic albumin/oleate concentrations oleate uptake by isolated hepatocytes, cardiac myocytes, and adipocytes is a saturable function of the unbound oleate concentration. Uptake kinetics are consistent with the conventional theory. *J Clin Invest.* 1989;84(4):1325-33.

3. Murota K, and Storch J. Uptake of micellar long-chain fatty acid and sn-2-monoacylglycerol into human intestinal Caco-2 cells exhibits characteristics of protein-mediated transport. *J Nutr.* 2005;135(7):1626-30.

4. Abumrad NA, and Goldberg IJ. CD36 actions in the heart: Lipids, calcium, inflammation, repair and more? *Biochim Biophys Acta.* 2016;1860(10):1442-9.

5. Silverstein RL, and Febbraio M. CD36, a scavenger receptor involved in immunity, metabolism, angiogenesis, and behavior. *Science signaling.* 2009;2(72):re3.

6. Endemann G, Stanton LW, Madden KS, Bryant CM, White RT, and Protter AA. CD36 is a receptor for oxidized low density lipoprotein. *J Biol Chem.* 1993;268(16):11811-6.

7. Abumrad NA, el-Maghrabi MR, Amri EZ, Lopez E, and Grimaldi PA. Cloning of a rat adipocyte membrane protein implicated in binding or transport of long-chain fatty acids that is induced during preadipocyte differentiation. Homology with human CD36. *J Biol Chem.* 1993;268(24):17665-8.

8. Hsieh FL, Turner L, Bolla JR, Robinson CV, Lavstsen T, and Higgins MK. The structural basis for CD36 binding by the malaria parasite. *Nature communications.* 2016;7:12837.

9. Nahle Z, Hsieh M, Pietka T, Coburn CT, Grimaldi PA, Zhang MQ, et al. CD36-dependent regulation of muscle FoxO1 and PDK4 in the PPAR delta/beta-mediated adaptation to metabolic stress. *J Biol Chem.* 2008;283(21):14317-26.

10. Samovski D, Sun J, Pietka T, Gross RW, Eckel RH, Su X, et al. Regulation of AMPK activation by CD36 links fatty acid uptake to beta-oxidation. *Diabetes.* 2015;64(2):353-9.

11. Coburn CT, Knapp FF, Jr., Febbraio M, Beets AL, Silverstein RL, and Abumrad NA. Defective uptake and utilization of long chain fatty acids in muscle and adipose tissues of CD36 knockout mice. *J Biol Chem.* 2000;275(42):32523-9.

12. Febbraio M, Abumrad NA, Hajjar DP, Sharma K, Cheng W, Pearce SF, et al. A null mutation in murine CD36 reveals an important role in fatty acid and lipoprotein metabolism. *J Biol Chem.* 1999;274(27):19055-62.

13. Drover VA, Ajmal M, Nassir F, Davidson NO, Nauli AM, Sahoo D, et al. CD36 deficiency impairs intestinal lipid secretion and clearance of chylomicrons from the blood. *J Clin Invest.* 2005;115(5):1290-7.

14. Nozaki S, Tanaka T, Yamashita S, Sohmiya K, Yoshizumi T, Okamoto F, et al. CD36 mediates long-chain fatty acid transport in human myocardium: complete myocardial accumulation defect of radiolabeled long-chain fatty acid analog in subjects with CD36 deficiency. *Mol Cell Biochem.* 1999;192(1-2):129-35.

15. Ma X, Bacci S, Mlynarski W, Gottardo L, Soccio T, Menzaghi C, et al. A common haplotype at the CD36 locus is associated with high free fatty acid levels and increased cardiovascular risk in Caucasians. *Human molecular genetics.* 2004;13(19):2197-205.

16. Hevener A, Reichart D, Janez A, and Olefsky J. Female rats do not exhibit free fatty acid-induced insulin resistance. *Diabetes.* 2002;51(6):1907-12.

17. Priego T, Sanchez J, Pico C, and Palou A. Sex-differential expression of metabolism-related genes in response to a high-fat diet. *Obesity (Silver Spring, Md).* 2008;16(4):819-26.

18. Masuda D, Hirano K, Oku H, Sandoval JC, Kawase R, Yuasa-Kawase M, et al. Chylomicron remnants are increased in the postprandial state in CD36 deficiency. *J Lipid Res.* 2009;50(5):999-1011.

19. Hajri T, Han XX, Bonen A, and Abumrad NA. Defective fatty acid uptake modulates insulin responsiveness and metabolic responses to diet in CD36-null mice. *J Clin Invest.* 2002;109(10):1381-9.

20. Lundsgaard AM, and Kiens B. Gender differences in skeletal muscle substrate metabolism - molecular mechanisms and insulin sensitivity. *Frontiers in endocrinology.* 2014;5:195.

21. Fukuchi K, Nozaki S, Yoshizumi T, Hasegawa S, Uehara T, Nakagawa T, et al. Enhanced myocardial glucose use in patients with a deficiency in long-chain fatty acid transport (CD36 deficiency). *J Nucl Med.* 1999;40(2):239-43.

22. Trent CM, Yu S, Hu Y, Skoller N, Huggins LA, Homma S, et al. Lipoprotein lipase activity is required for cardiac lipid droplet production. *J Lipid Res.* 2014;55(4):645-58.

23. Liu L, Shi X, Choi CS, Shulman GI, Klaus K, Nair KS, et al. Paradoxical coupling of triglyceride synthesis and fatty acid oxidation in skeletal muscle overexpressing DGAT1. *Diabetes.* 2009;58(11):2516-24.

24. Monetti M, Levin MC, Watt MJ, Sajan MP, Marmor S, Hubbard BK, et al. Dissociation of hepatic steatosis and insulin resistance in mice overexpressing DGAT in the liver. *Cell Metab.* 2007;6(1):69-78.

25. Ibrahimi A, Bonen A, Blinn WD, Hajri T, Li X, Zhong K, et al. Muscle-specific overexpression of FAT/CD36 enhances fatty acid oxidation by contracting muscle, reduces

plasma triglycerides and fatty acids, and increases plasma glucose and insulin. *J Biol Chem.* 1999;274(38):26761-6.

26.   Nickerson JG, Alkhateeb H, Benton CR, Lally J, Nickerson J, Han XX, et al. Greater transport efficiencies of the membrane fatty acid transporters FAT/CD36 and FATP4 compared with FABPpm and FATP1 and differential effects on fatty acid esterification and oxidation in rat skeletal muscle. *J Biol Chem.* 2009;284(24):16522-30.

27.   Coort SL, Willems J, Coumans WA, van der Vusse GJ, Bonen A, Glatz JF, et al. Sulfo-N-succinimidyl esters of long chain fatty acids specifically inhibit fatty acid translocase (FAT/CD36)-mediated cellular fatty acid uptake. *Mol Cell Biochem.* 2002;239(1-2):213-9.

28.   Jay AG, Chen AN, Paz MA, Hung JP, and Hamilton JA. CD36 binds oxidized low density lipoprotein (LDL) in a mechanism dependent upon fatty acid binding. *J Biol Chem.* 2015;290(8):4590-603.

29.   Bartelt A, Bruns OT, Reimer R, Hohenberg H, Ittrich H, Peldschus K, et al. Brown adipose tissue activity controls triglyceride clearance. *Nat Med.* 2011;17(2):200-5.

30.   Kanda T, Brown JD, Orasanu G, Vogel S, Gonzalez FJ, Sartoretto J, et al. PPARgamma in the endothelium regulates metabolic responses to high-fat diet in mice. *J Clin Invest.* 2009;119(1):110-24.

31.   Coppiello G, Collantes M, Sirerol-Piquer MS, Vandenwijngaert S, Schoors S, Swinnen M, et al. Meox2/Tcf15 heterodimers program the heart capillary endothelium for cardiac fatty acid uptake. *Circulation.* 2015;131(9):815-26.

32.   Hagberg CE, Mehlem A, Falkevall A, Muhl L, Fam BC, Ortsater H, et al. Targeting VEGF-B as a novel treatment for insulin resistance and type 2 diabetes. *Nature.* 2012;490(7420):426-30.

33.   Kivela R, Bry M, Robciuc MR, Rasanen M, Taavitsainen M, Silvola JM, et al. VEGF-B-induced vascular growth leads to metabolic reprogramming and ischemia resistance in the heart. *EMBO Mol Med.* 2014;6(3):307-21.

34.   Jang C, Oh SF, Wada S, Rowe GC, Liu L, Chan MC, et al. A branched-chain amino acid metabolite drives vascular fatty acid transport and causes insulin resistance. *Nat Med.* 2016;22(4):421-6.

35.   Salameh A, Daquinag AC, Staquicini DI, An Z, Hajjar KA, Pasqualini R, et al. Prohibitin/annexin 2 interaction regulates fatty acid transport in adipose tissue. *JCI insight.* 2016;1(10).

36.   Nolan DJ, Ginsberg M, Israely E, Palikuqi B, Poulos MG, James D, et al. Molecular signatures of tissue-specific microvascular endothelial cell heterogeneity in organ maintenance and regeneration. *Developmental cell.* 2013;26(2):204-19.

37.   Glatz JF, Nabben M, Heather LC, Bonen A, and Luiken JJ. Regulation of the subcellular trafficking of CD36, a major determinant of cardiac fatty acid utilization. *Biochim Biophys Acta.* 2016;1860(10):1461-71.

38.   Angin Y, Steinbusch LK, Simons PJ, Greulich S, Hoebers NT, Douma K, et al. CD36 inhibition prevents lipid accumulation and contractile dysfunction in rat cardiomyocytes. *Biochem J.* 2012;448(1):43-53.

39.   Sung MM, Byrne NJ, Kim TT, Levasseur J, Masson G, Boisvenue JJ, et al. Cardiomyocyte-specific ablation of CD36 accelerates the progression from compensated cardiac hypertrophy to heart failure. *Am J Physiol Heart Circ Physiol.* 2017;312(3):H552-H60.

40.   Guerre-Millo M, Rouault C, Poulain P, Andre J, Poitout V, Peters JM, et al. PPAR-alpha-null mice are protected from high-fat diet-induced insulin resistance. *Diabetes.* 2001;50(12):2809-14.

41.   Kotani K, Peroni OD, Minokoshi Y, Boss O, and Kahn BB. GLUT4 glucose transporter deficiency increases hepatic lipid production and peripheral lipid utilization. *J Clin Invest.* 2004;114(11):1666-75.

42.   Tordjman K, Bernal-Mizrachi C, Zemany L, Weng S, Feng C, Zhang F, et al. PPARalpha deficiency reduces insulin resistance and atherosclerosis in apoE-null mice. *J Clin Invest.* 2001;107(8):1025-34.

43.   Augustus A, Yagyu H, Haemmerle G, Bensadoun A, Vikramadithyan RK, Park SY, et al. Cardiac-specific knock-out of lipoprotein lipase alters plasma lipoprotein triglyceride metabolism and cardiac gene expression. *J Biol Chem.* 2004;279(24):25050-7.

44.   Lepretre F, Linton KJ, Lacquemant C, Vatin V, Samson C, Dina C, et al. Genetic study of the CD36 gene in a French diabetic population. *Diabetes Metab.* 2004;30(5):459-63.

45.   Miyaoka K, Kuwasako T, Hirano K, Nozaki S, Yamashita S, and Matsuzawa Y. CD36 deficiency associated with insulin resistance. *Lancet.* 2001;357(9257):686-7.

46.   Kuang M, Febbraio M, Wagg C, Lopaschuk GD, and Dyck JR. Fatty acid translocase/CD36 deficiency does not energetically or functionally compromise hearts before or after ischemia. *Circulation.* 2004;109(12):1550-7.

47.   Nagendran J, Pulinilkunnil T, Kienesberger PC, Sung MM, Fung D, Febbraio M, et al. Cardiomyocyte-specific ablation of CD36 improves post-ischemic functional recovery. *J Mol Cell Cardiol.* 2013;63:180-8.

48.   Irie H, Krukenkamp IB, Brinkmann JF, Gaudette GR, Saltman AE, Jou W, et al. Myocardial recovery from ischemia is impaired in CD36-null mice and restored by myocyte CD36 expression or medium-chain fatty acids. *Proceedings of the National Academy of Sciences of the United States of America.* 2003;100(11):6819-24.

49. Goldberg IJ, Trent CM, and Schulze PC. Lipid metabolism and toxicity in the heart. *Cell Metab.* 2012;15(6):805-12.

50. Lopaschuk GD, Ussher JR, Folmes CD, Jaswal JS, and Stanley WC. Myocardial fatty acid metabolism in health and disease. *Physiological reviews.* 2010;90(1):207-58.

51. Howard MD, Hood ED, Greineder CF, Alferiev IS, Chorny M, and Muzykantov V. Targeting to endothelial cells augments the protective effect of novel dual bioactive antioxidant/anti-inflammatory nanoparticles. *Mol Pharm.* 2014;11(7):2262-70.

52. Folch J, Lees M, and Sloane Stanley GH. A simple method for the isolation and purification of total lipides from animal tissues. *J Biol Chem.* 1957;226(1):497-509.

53. Seo T, Al-Haideri M, Treskova E, Worgall TS, Kako Y, Goldberg IJ, et al. Lipoprotein lipase-mediated selective uptake from low density lipoprotein requires cell surface proteoglycans and is independent of scavenger receptor class B type 1. *J Biol Chem.* 2000;275(39):30355-62.

54. Louch WE, Sheehan KA, and Wolska BM. Methods in cardiomyocyte isolation, culture, and gene transfer. *J Mol Cell Cardiol.* 2011;51(3):288-98.

55. Riches AC, Sharp JG, Thomas DB, and Smith SV. Blood volume determination in the mouse. *J Physiol.* 1973;228(2):279-84.

56. Burkart EM, Sambandam N, Han X, Gross RW, Courtois M, Gierasch CM, et al. Nuclear receptors PPARbeta/delta and PPARalpha direct distinct metabolic regulatory programs in the mouse heart. *J Clin Invest.* 2007;117(12):3930-9.
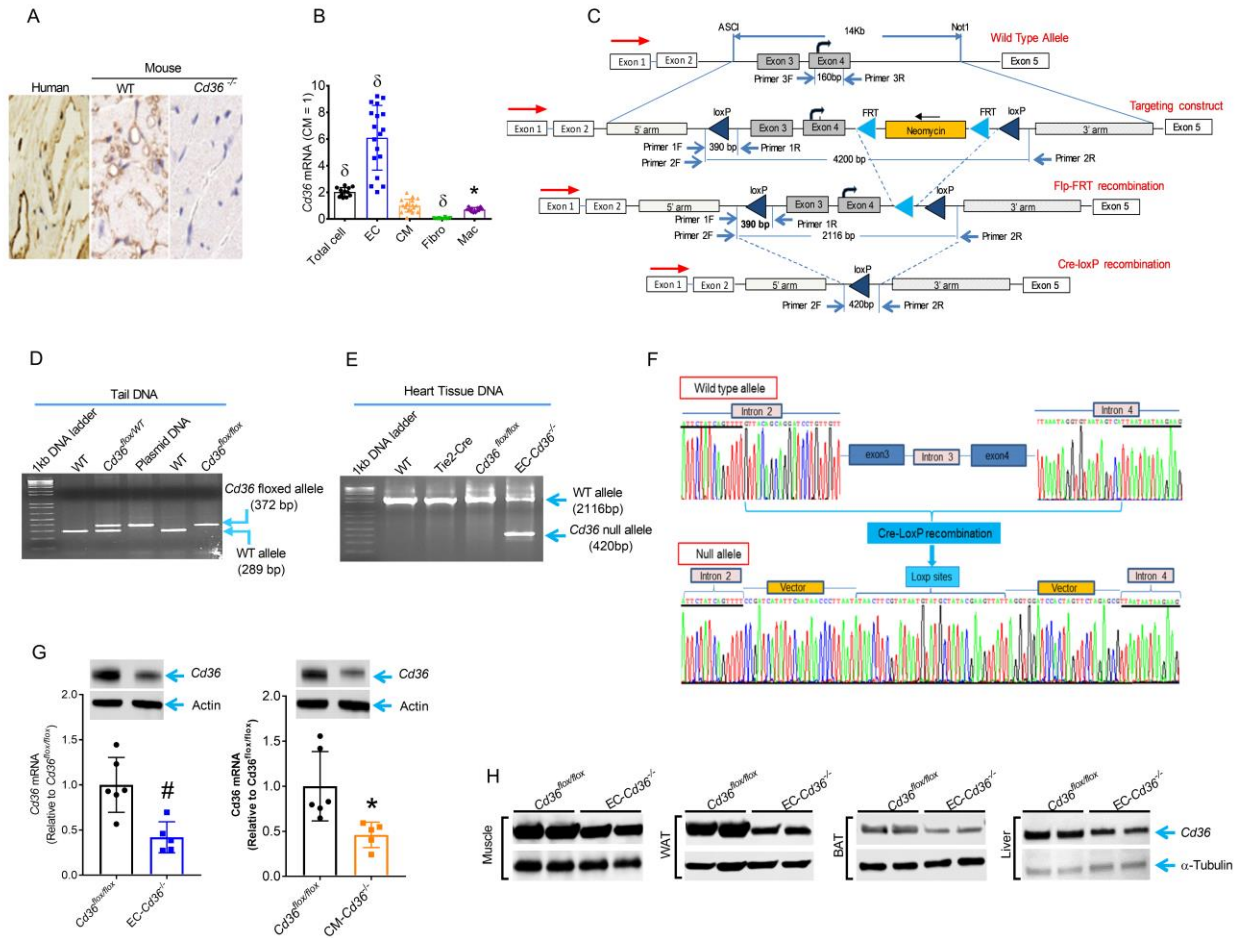
Fig. 1: CD36 distribution in human and mouse hearts and creation of EC- and CM-*Cd36*^{-/-} mice. (A) CD36 antibody staining in CMs and blood vessel ECs of human and mouse hearts. **(B)** Male mouse heart sub-organ fractionation showing CD36 mRNA levels in different cell types (n=12-18). Data are mean ratios normalized to CM-*Cd36*^{-/-} (set as 1.0). **(C)** Genomic structure of murine *Cd36*, the targeting vector, and mutated allele. Brown boxes represent numbered murine *Cd36* exons. Red arrows indicate transcription orientation. Black bent arrows indicate the translation start site. PCR primers (blue arrows) were chosen to differentiate between the WT genomic allele and homologously recombined allele. **(D)** PCR of tail genomic DNA (using primer 1) and **(E)** heart tissue DNA (using primer 2) from *Cd36*^{flox/flox}, EC-*Cd36*^{-/-}, and CM-*Cd36*^{-/-} mice. **(F)** PCR product sequencing showing ablation of exons 3 and 4 of *Cd36* gene after Cre-mediated recombination. **(G)** Heart CD36 mRNA in EC-*Cd36*^{-/-} (left) and CM-*Cd36*^{-/-} (right) mice quantified by qRT-PCR using primer 3 (n=5-6, mean ± SD). Data are corrected for 18S rRNA and normalized to Cd36flox/flox controls. **Insert:** Immunoblot of CD36 in EC-*Cd36*^{-/-} and CM-*Cd36*^{-/-} mouse hearts. **(H)** Immunoblot of CD36 in EC-*Cd36*^{-/-} muscle, WAT, BAT, and liver. *P< 0.05, #P < 0.01 and δP < 0.001 compared to *Cd36*^{flox/flox} controls. P values were calculated by one-way ANOVA with a Dunnett's multiple comparisons test.
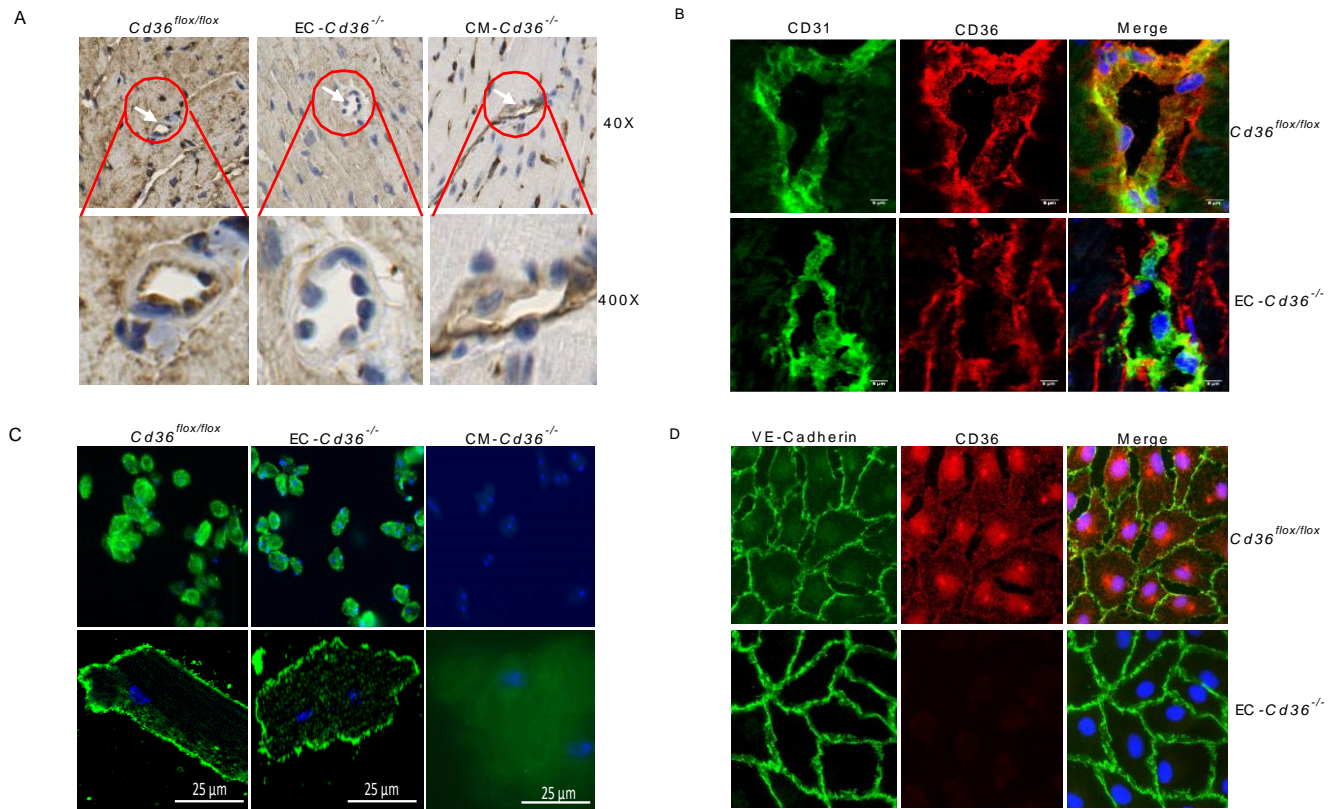
Fig. 2: Immunocytochemistry/ Immunofluorescence staining of heart tissues and isolated ECs and CMs. (A) CD36 staining from $Cd36^{flox/flox}$, EC-$Cd36^{-/-}$, and CM-$Cd36^{-/-}$ hearts (upper). Magnified CD36 staining in vascular endothelium and CMs (bottom). (**B**) $Cd36^{flox/flox}$ and EC-$Cd36^{-/-}$ heart sections double-stained with anti-CD31 (green) and anti-CD36 (red) antibodies. **(C)** Images of isolated CMs from $Cd36^{flox/flox}$, EC-$Cd36^{-/-}$ and CM-$Cd36^{-/-}$ mice hearts stained with anti-CD36 antibody. **(D)** Images of isolated ECs from $Cd36^{flox/flox}$ and EC-$Cd36^{-/-}$ mice stained with anti-VE-cadherin (green) and anti-CD36 (red) antibodies.
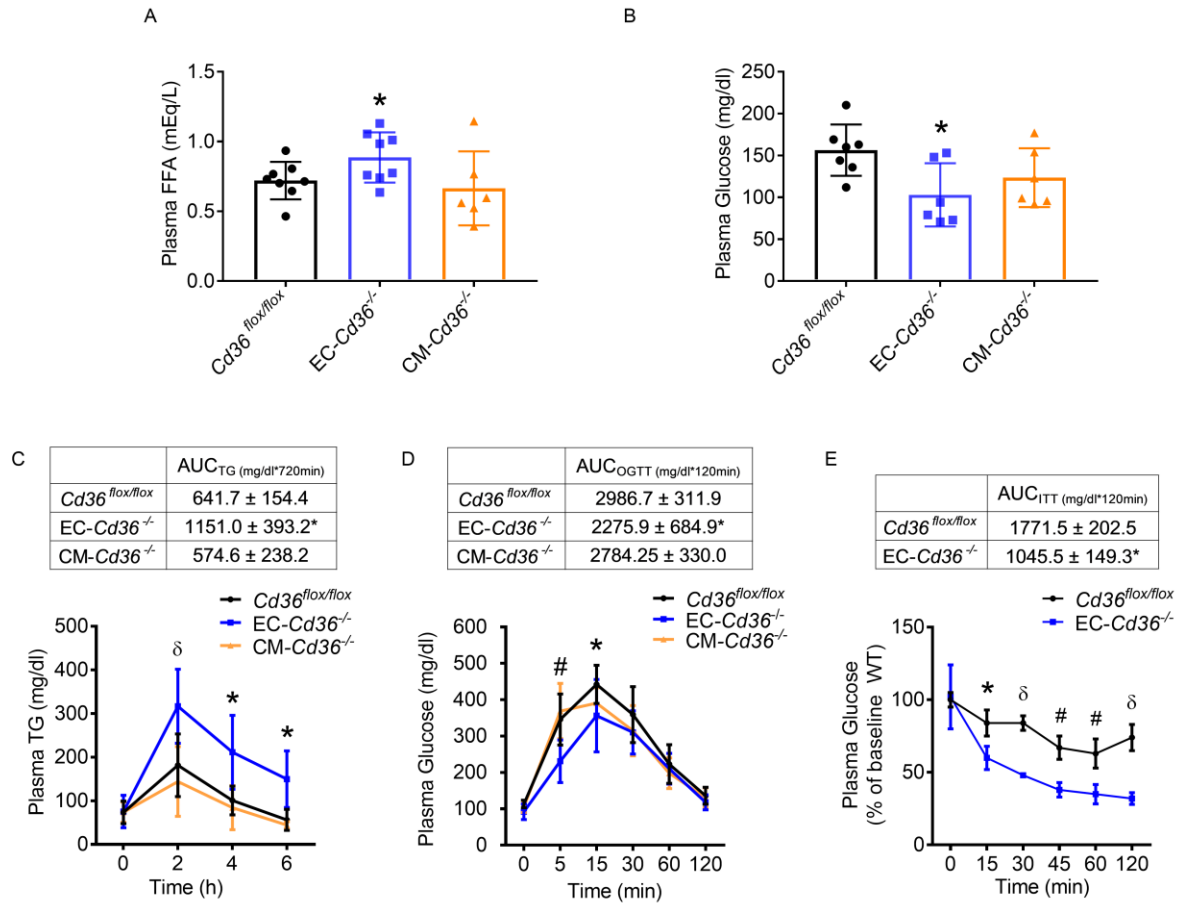
A

B

C

	AUC$_{TG}$ (mg/dl*720min)
$Cd36^{flox/flox}$	641.7 ± 154.4
EC-$Cd36^{-/-}$	1151.0 ± 393.2*
CM-$Cd36^{-/-}$	574.6 ± 238.2

D

	AUC$_{OGTT}$ (mg/dl*120min)
$Cd36^{flox/flox}$	2986.7 ± 311.9
EC-$Cd36^{-/-}$	2275.9 ± 684.9*
CM-$Cd36^{-/-}$	2784.25 ± 330.0

E

	AUC$_{ITT}$ (mg/dl*120min)
$Cd36^{flox/flox}$	1771.5 ± 202.5
EC-$Cd36^{-/-}$	1045.5 ± 149.3*

Fig. 3: EC-$Cd36^{-/-}$ mice have increased FFA and postprandial TG levels but improved glucose metabolism. (A) Plasma FFA in 4-month-old male mice fasted for 16 h (n=6-8). **(B)** Plasma glucose levels (n=6-7) in $Cd36^{flox/flox}$, EC-$Cd36^{-/-}$, and CM-$Cd36^{-/-}$ mice. **(C)** Postprandial TG response in $Cd36^{flox/flox}$, EC-$Cd36^{-/-}$, and CM-$Cd36^{-/-}$ mice. Plasma TG concentration was measured at 0, 2, 4, and 6 h after intragastric administration of olive oil (n=5-7). **Insert:** Area under curve (AUC) for postprandial TGs. **(D)** 4-month-old male mice (n=4-8) were fasted for 16 h before oral glucose administration. Tail blood was collected for glucose measurements at 0, 15, 30, 60, and 120 min. **Insert**: AUC of glucose excursions. **(E)** Insulin tolerance test: Mice (n=4-5, data representative of two independent experiments) were fasted for 4 h and given insulin IP, 0.75 U/kg body weight. Tail blood samples were obtained before insulin administration (time-zero) and then at 15, 30, 45, 60, and 120 min after insulin. Data are shown as mean ± SD. *P < 0.05, #P < 0.01 and δ P < 0.001 compared to $Cd36^{flox/flox}$ controls. P values were calculated using one-way ANOVA with a Dunnett's multiple comparisons test.
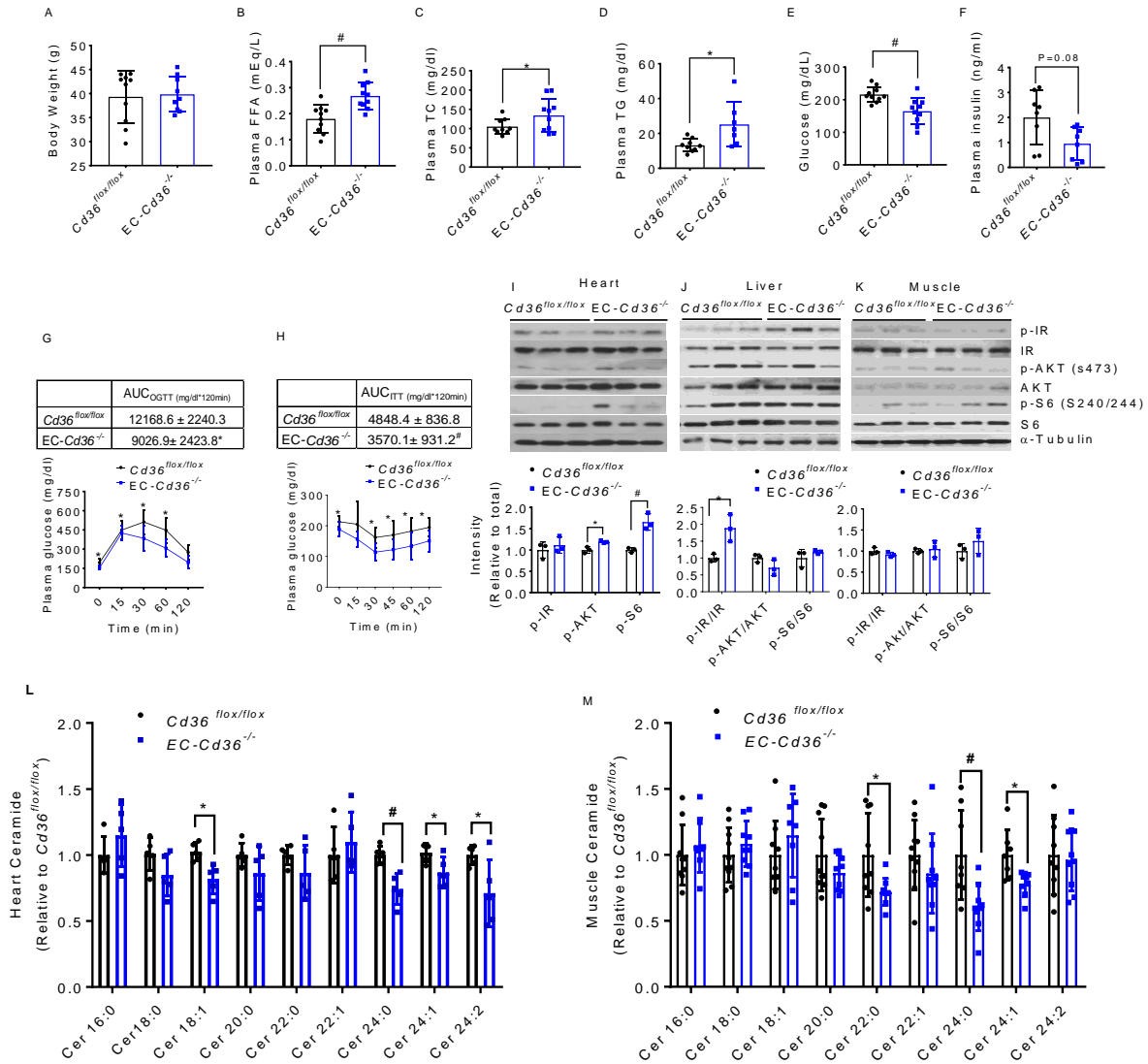
Fig. 4: EC-*Cd36*^{-/-} improved glucose homeostasis and increased insulin sensitivity in 6-month-old male mice fed high fat diet (HFD) for 4 months. (A-E) Body weight, plasma lipids, and glucose after 16 h fast. **(F)** Plasma insulin after 16 h fast then 4 h refeeding. **(G)** Glucose tolerance: Male mice fasted for 16 h were given oral glucose, and tail blood samples were collected for glucose measurements at 0, 15, 30, 60, and 120 min. **Insert**: AUC of glucose excursions. **(H)** Insulin tolerance test: mice fasted for 4 h were given insulin IP, 0.75 U/kg body weight. Tail blood samples were obtained at time-zero and then at 15, 30, 45, 60 and 120 min after insulin administration. **(I)** Activity of IR, AKT, and S6 in *Cd36*[flox/flox] and EC-*Cd36*^{-/-} mice after 20 min insulin injection with densitometric analysis in heart, (**J**) liver, and (**K**) skeletal muscle. **(L, M)** Individual ceramide species in heart (n=5) and muscle (n=9-10). Data are shown as mean ± SD. *P < 0.05 and #P < 0.01 compared to *Cd36*[flox/flox] controls. P values were calculated using one-way ANOVA with a Dunnett's multiple comparisons test.
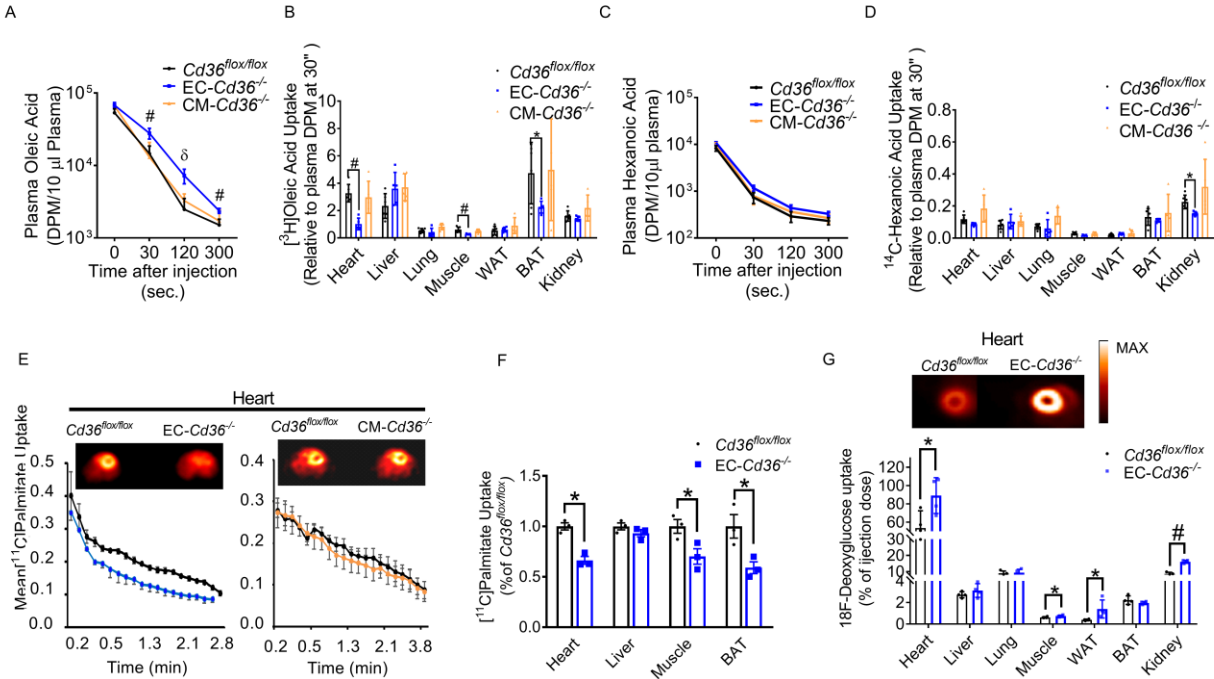
Fig. 5: EC-*Cd36*^{-/-} mice have reduced tissue LCFA uptake during fasting. (A-D) Uptake of oleic and hexanoic acids in EC-*Cd36*^{-/-} mice. 4-month-old mice were fasted for 16 h and given a tail IV injection of [³H]oleic acid and [¹⁴C]hexanoic acid. **(A)** Plasma ³H radioactivity in *Cd36*^{flox/flox}, EC-*Cd36*^{-/-}, and CM-*Cd36*^{-/-} mice (n=5-6) measured at the indicated times after the injection. **(B)** ³H content of different tissues **(C)** Plasma ¹⁴C radioactivity and **(D)** ¹⁴C content of different tissues. **(E)** Real time [¹¹C]palmitic acid uptake into heart and **(F)** tissue [¹¹C]palmitic acid uptake in *Cd36*^{flox/flox} and EC–*Cd36*^{-/-} male mice (n=4). **(G)** Tissue [¹⁸F]DG uptake in *Cd36*^{flox/flox} and EC–*Cd36*^{-/-} mice (n=4) derived from summing uptake kinetics up to 60 min post-tracer administration. **Insert**: representative scans of FDG accumulation at 60 min by hearts of control and EC-*Cd36*^{-/-} hearts from 16 h fasted mice. Data are shown as mean ± SD. *P < 0.05, #P < 0.01 and δP < 0.001 compared to *Cd36*^{flox/flox} controls. P values were calculated using one-way ANOVA with a Dunnett's multiple comparisons test.
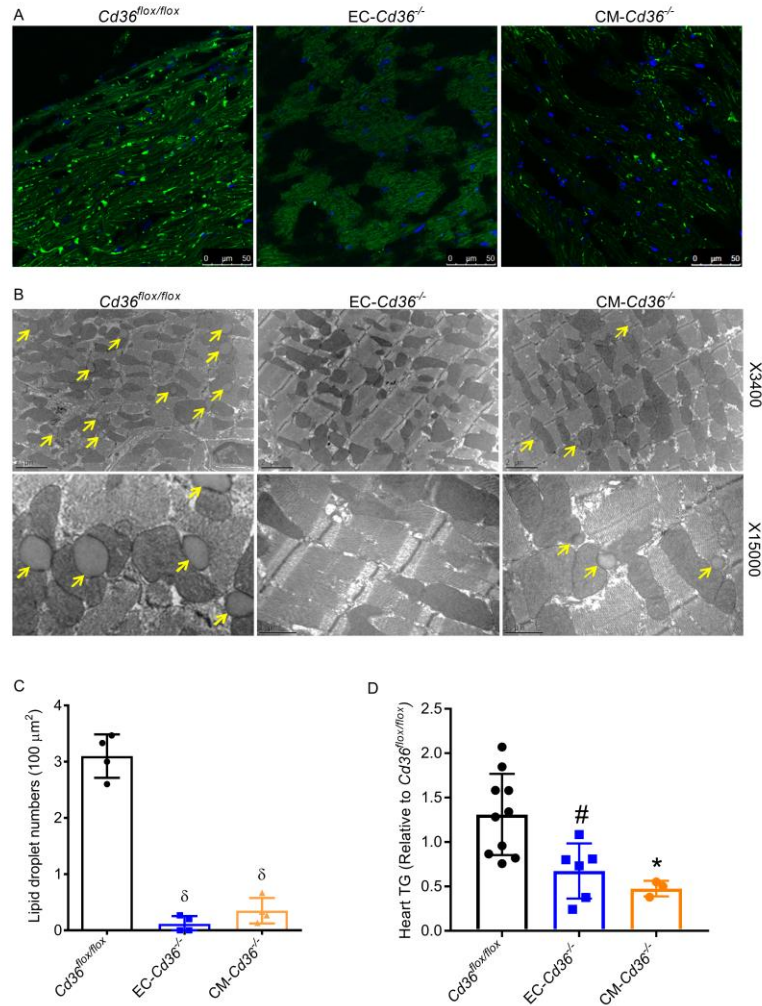
Fig. 6: CD36 deletion in ECs or CMs reduces heart lipid storage during fasting. (A) Heart tissue section from *Cd36^flox/flox^*, EC-*Cd36^-/-^*, and CM-*Cd36^-/-^* mice stained with BODIPY 493/503**. (B)** Electron micrographs (original magnification ×3,400 and ×15,000) of myocardial tissue showing a significant decrease in lipid droplets within the sarcoplasm of CMs in both EC-*Cd36^-/-^* and CM-*Cd36^-/-^* mice. The yellow arrow indicates a lipid droplet. **(C)** Lipid droplet number in heart tissue sections (n=4) of *Cd36^flox/flox^*, EC-*Cd36^-/-^*, and CM-*Cd36^-/-^* mice expressed per 100 μm². **(D)** Heart TG content in *Cd36^flox/flox^* (n=10), EC-*Cd36^-/-^* (n=6), and CM-*Cd36^-/-^* mice (n=3). Data are shown as mean ± SD. *P < 0.05 and δP < 0.001 compared to *Cd36^flox/flox^* controls. P values were calculated using one-way ANOVA with a Dunnett's multiple comparisons test.
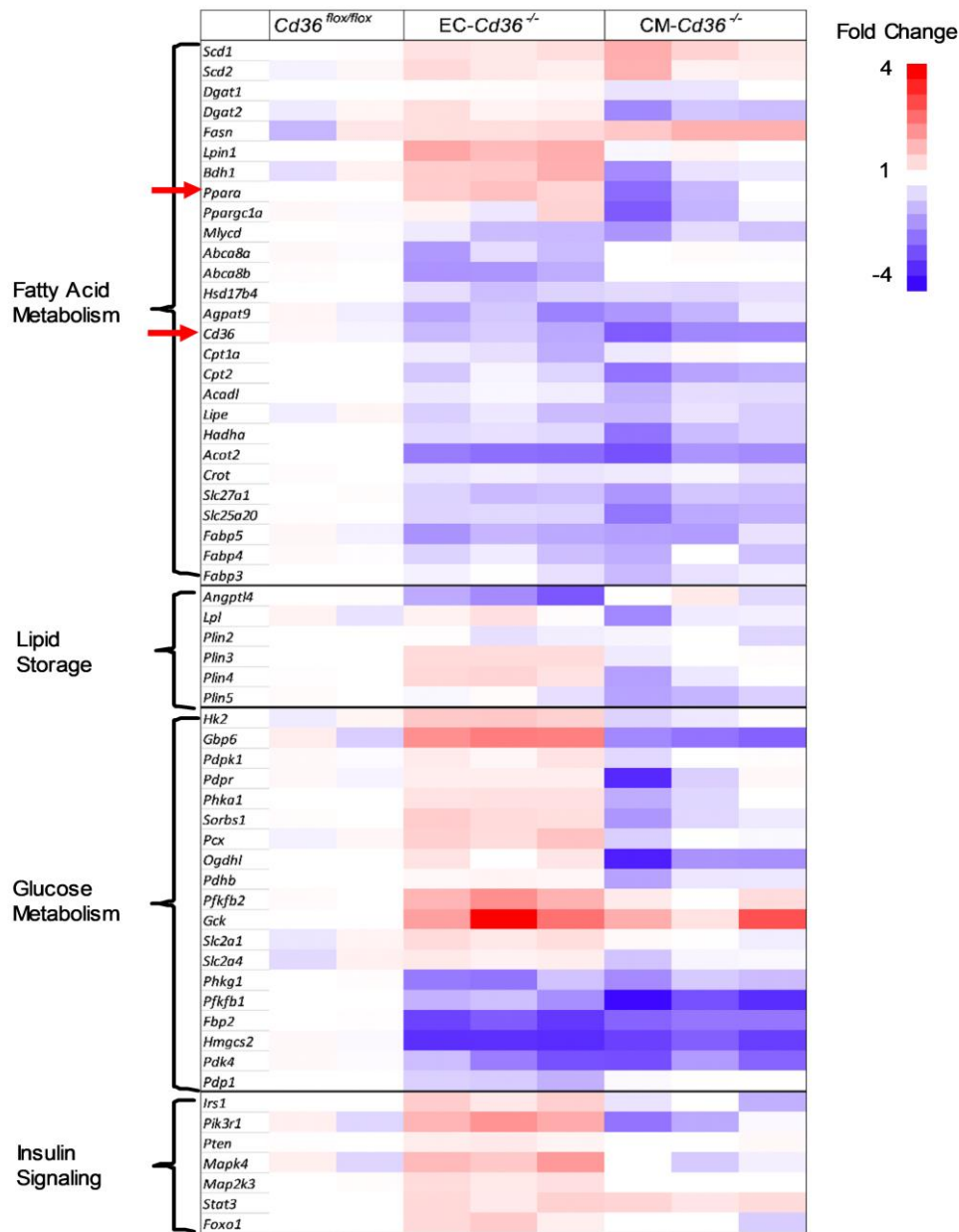
Fig. 7: Heart tissue mRNA expression in mice with EC or CM *Cd36* deletion. Clustered heat maps from RNA-Seq data showing differential expression profiles for *Cd36^flox/flox^*, EC-*Cd36^-/-^*, and CM-*Cd36^-/-^* mice. Red indicates over-abundant expression and blue indicates under-abundant expression.
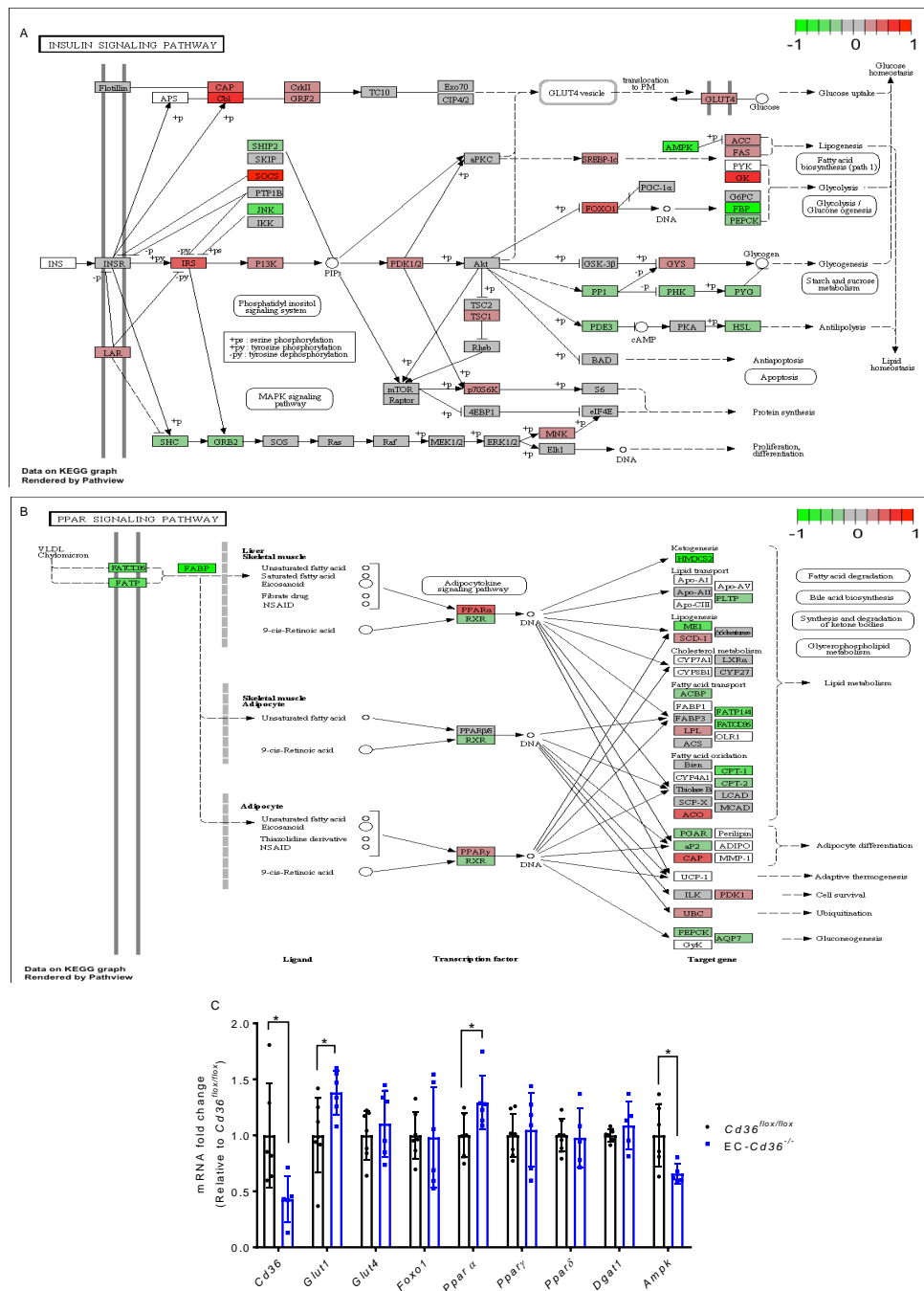
Fig. 8: KEGG analysis of insulin signaling and PPAR pathways. (A) KEGG analysis of insulin and **(B)** PPAR signaling pathways. **(C)** qRT-PCR analysis of heart mRNA in *Cd36$^{flox/flox}$*, EC-*Cd36$^{-/-}$*, and CM-*Cd36$^{-/-}$* mice (n=5-7). Data are shown as mean ± SD. *P < 0.05 compared to *Cd36$^{flox/flox}$* controls. P values were calculated using one-way ANOVA with a Dunnett's multiple comparisons test.